Electronic Supplementary Material (ESI) for Analytical Methods.

Electronic Supporting Material
for
Acetylcholinesterase-$Cu_3(PO_4)_2$ hybrid nanoflowers for electrochemical detection of dichlorvos using square-wave voltammetry

Limin Yang,[a,*] Xiaolong Zhang,[a,¶] Mingming Li,[a,¶] Linjiao Qu,[a] and Zhen Liu[b,*]

[a]State Key Laboratory of Heavy Oil Processing and Center for Bioengineering and Biotechnology, China University of Petroleum (East China), Qingdao, China

[b]Institute of Biomedical Engineering, Shenzhen Bay Laboratory, Shenzhen, China

¶These authors contributed equally to this work and should be considered co-second authors.

*Correspondence: yanglimin@upc.edu.cn (Limin Yang) and liuzhen@szbl.ac.cn

This material includes:

References

1. Characterization of GO

The GO was characterized by XRD and FT-IR. The XRD pattern of GO was shown in **Figure S1A**. The diffractogram shows a characteristically strong peak of GO at 11.38° (2θ).[1] There is also a weak and broad diffraction peak that appears at 21.62° (2θ), indicating the presence of unoxidized graphite residues.[2] FT-IR spectrum of GO obtained from the KBr pellet is shown in **Figure S1B**. The spectrum shows a strong and broad absorption at 3195 cm^{-1} due to the O-H stretching vibration.[3] The C=O stretching peak is observed at 1731 cm^{-1} and the peak at 1618 cm^{-1} may be attributed to adsorbed water molecules or the carbon skeleton vibrations of graphene. The peak at 1226 cm^{-1} represents the stretching of C-O-C and the peak at 1052 cm^{-1} corresponds to C-O groups.[4]

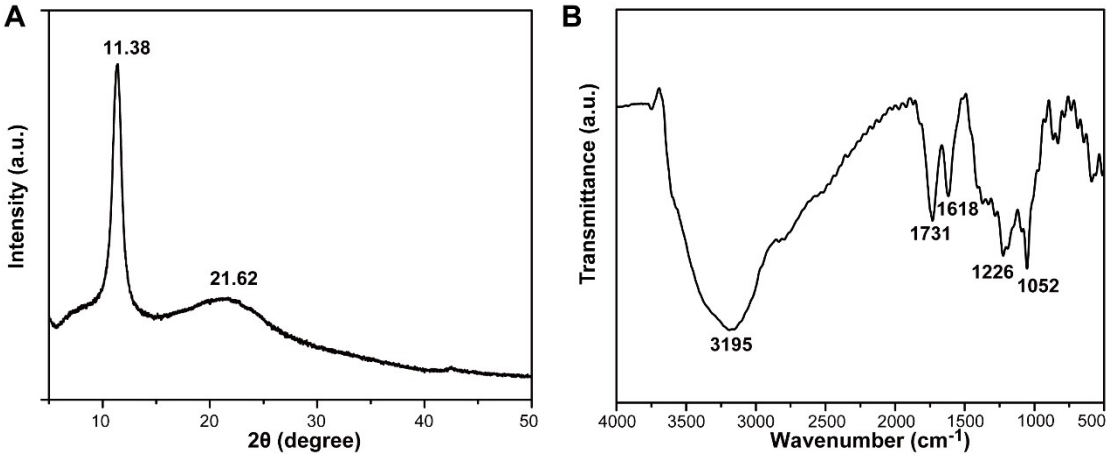

Figure S1 (A) XRD pattern and (B) FT-IR spectrum of GO.

2. Synthesis and characterization of AuNPs

The AuNPs were synthesized by the sodium citrate method. Briefly, 100 mL of 250 μM $HAuCl_4$ solution was heated to boiling under constant stirring. Rapidly, 2 mL of 0.34 M citrate solution was added. After heating for about 7 min, the color of the solution changed from light yellow to wine red, and then the heating was stopped. After the solution was cooled to room temperature with continuous stirring, the AuNP colloidal solution was prepared.

The AuNPs as prepared were characterized by UV-vis spectroscopy (UV-8000, Metash, China), transmission electron microscopy (TEM, JEM-2100UHR, JEOL, Japan), and zeta potential (NanoS, Malvern, England). The UV-visible spectrum shows the presence of a broad absorption band in the visible region at 520 nm (**Figure S2A**), corresponding to the surface plasmon band of AuNP. The TEM image (**Figure S2B**) clearly shows the existence of well-separated spherical nanoparticles with a diameter of 32.73 ± 6.8 nm. The zeta potential of AuNP is measured to be -41.2 mV (**Figure S2C**). It confirmed the formation of negative charges on the surface of AuNPs due to the citrate capping.

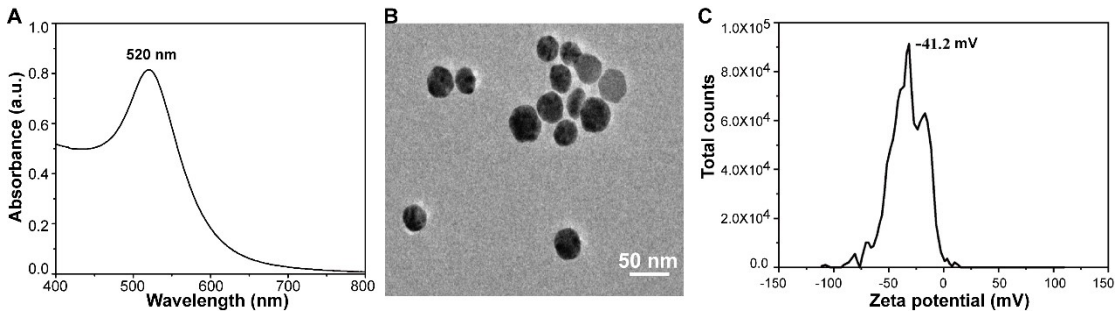

Figure S2 Characterization of AuNPs.

3. Fabrication of the AChE-$Cu_3(PO_4)_2$ HNF/AuNP/GO/GCE

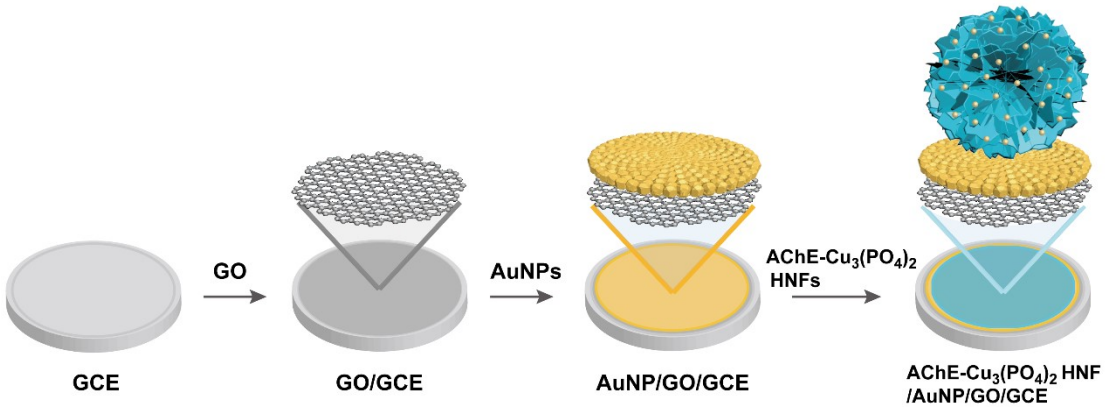

Figure S3 Schematic illustration of the fabrication of AChE-$Cu_3(PO_4)_2$ HNF/AuNP/GO/GCE.

4. SEM characterization of $Cu_3(PO_4)_2$ nanosheets

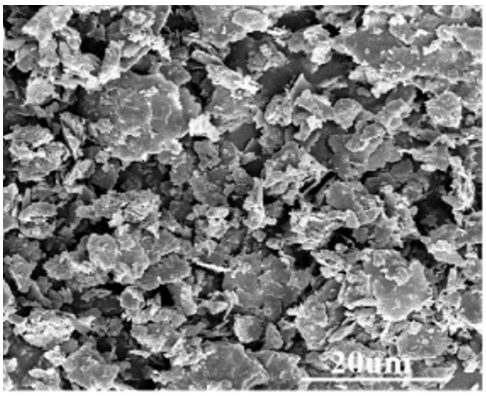

Figure S4 The SEM image of the nucleation of $Cu_3(PO_4)_2$ nanosheets.

5. XRD and FT-IR characterization of the AChE-$Cu_3(PO_4)_2$ HNFs

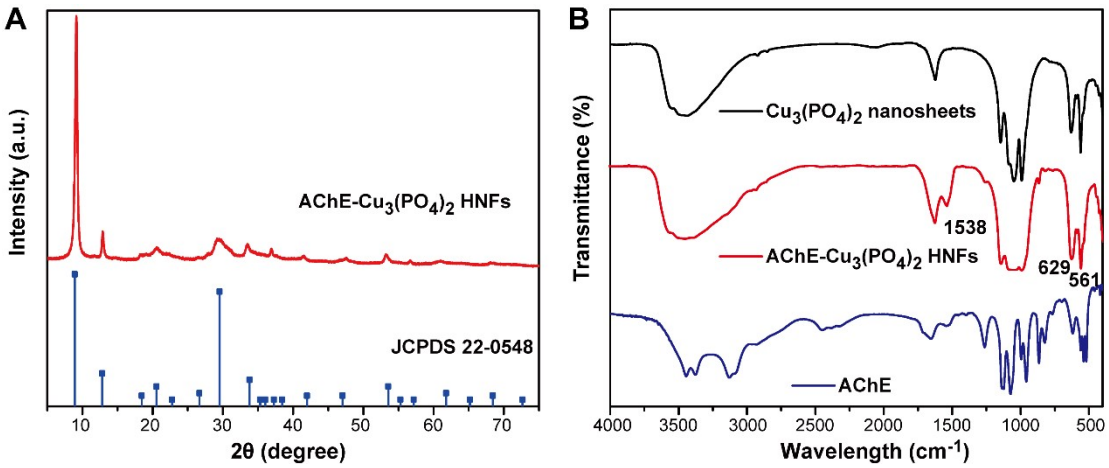

Figure S5 (A) XRD pattern and (B) FT-IR spectrum of the AChE-$Cu_3(PO_4)_2$ HNFs.

6. Steady-state kinetic study of the AChE/$Cu_3(PO_4)_2$-HNFs

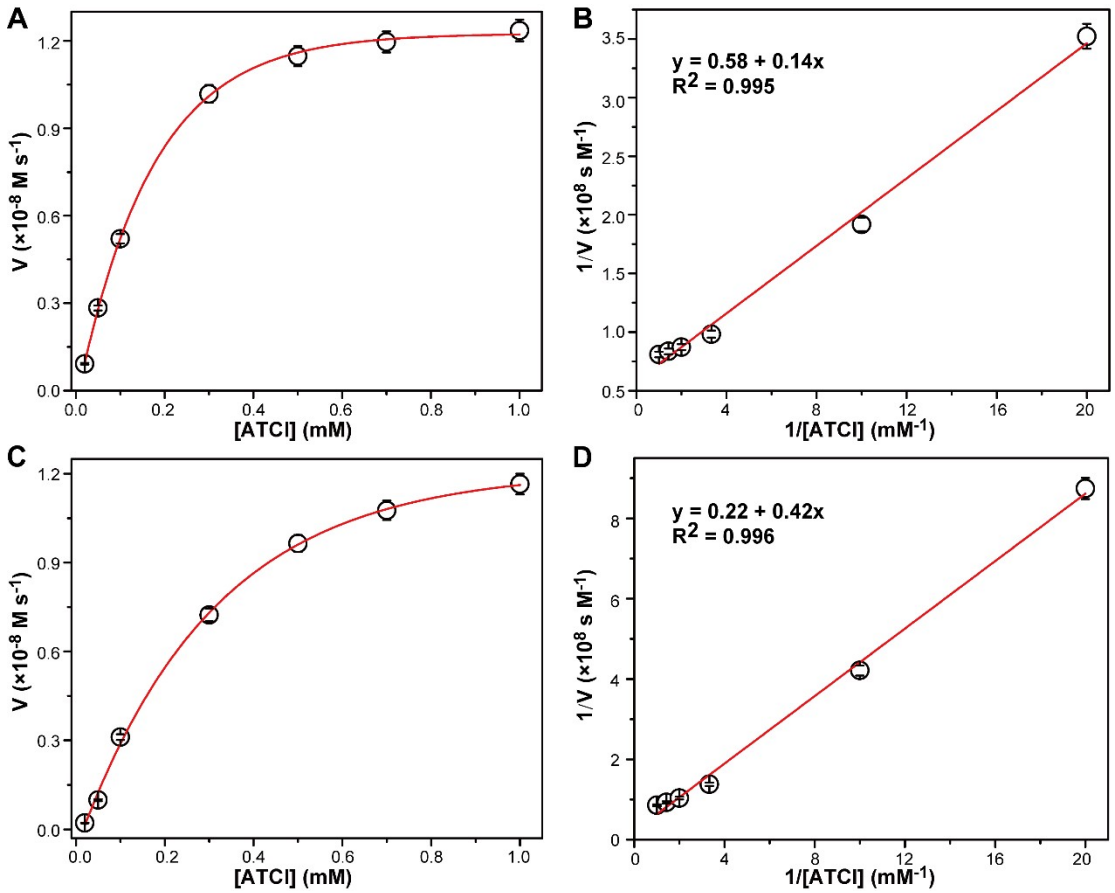

Figure S6 The steady-state kinetics analysis of the AChE/$Cu_3(PO_4)_2$-HNFs and the free AChE. Michaelis-Menten curves of the AChE/$Cu_3(PO_4)_2$-HNFs (A) or the free AChE (C) toward ATCl. The Lineweaver-Burk plots of the AChE/$Cu_3(PO_4)_2$-HNFs (B) or the free AChE (D) for ATCl.

7. Cyclic voltammograms for different modified electrodes

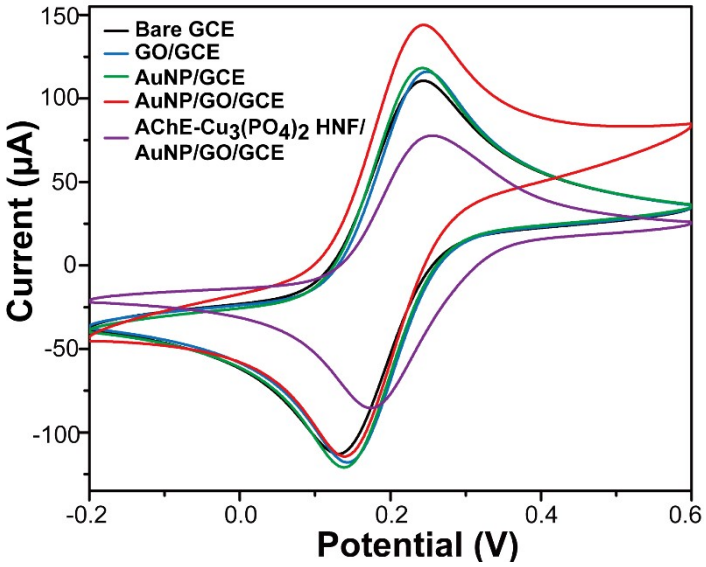

Figure S7 Cyclic voltammograms obtained in 5 mM $[Fe(CN)_6]^{3-/4-}$ (1:1) PBS containing 0.1 M KCl at different modified electrodes.

8. Control experimental data

As shown in **Figure S8**, dichlorvos could not produce any SWV signal even at a concentration of 1 mM (curves a-d). This indicates that dichlorvos itself does not present any oxidation or reduction peaks. Then, the SWV response of PBS was examined with the bare electrode (curve e) and enzyme-containing electrode (*i.e.*, AChE-$Cu_3(PO_4)_2$ HNF/AuNP/GO/GCE) (curve f), respectively. As illustrated in **Figure S8**, the PBS buffer caused a slight drift of the response signal, forming a background signal, regardless of the electrode surface modification. However, these influences are very small compared to the SWV signal brought by ATCl (curve g). Therefore, it is presumed that both the main and shoulder peaks should come from the oxidation reaction of the products generated by AChE-catalyzed ATCl hydrolysis on the electrode surface.

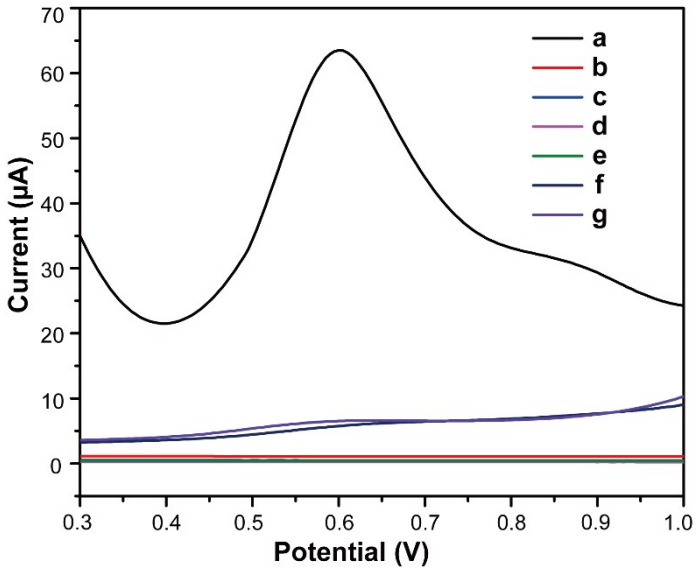

Figure S8 Comparison of the SWV response obtained from the control experiments (curves a-d: response of AuNP/GO/GCE to dichlorvos at different concentrations: a, 100 pM, b, 100 nM, c, 100 μM, and d, 1 mM; response to PBS by bare GCE (curve e) and AChE-$Cu_3(PO_4)_2$ HNF/AuNP/GO/GCE (curve f)) with that of the AChE-$Cu_3(PO_4)_2$ HNF/AuNP/GO/GCE to ATCl in PBS (curve g).

9. Calibration plot for the Ellman method

Briefly, after reacting the free AChE (1 mg mL^{-1}) with dichlorvos at different concentrations (0, 10 pM, 100 pM, 1 nM, 10 nM, and 100 nM) for 10 min, 200 µl of the reaction solution was taken and mixed with 200 µl of 20 mM DTNB, 100 µl of 40 mM ATCl, and 2.5 ml of water. After 30 min of reaction, the absorbance at 412 nm was measured. The inhibition rate (I' %) of dichlorvos was calculated using the following equation:

$$I'\,\% = (A_0 - A_i) / A_0 \times 100\,\% \quad (1)$$

where A_0 and A_i represent the absorbance at 412 nm of the AChE before and after exposure to dichlorvos, respectively. The calibration curve was obtained by plotting the I' % against the logarithm of concentration of dichlorvos (**Figure S9**). The calibration equation is I' % = 8.32 × log[dichlorvos] + 33.60 with a correlation coefficient (R^2) of 0.996.

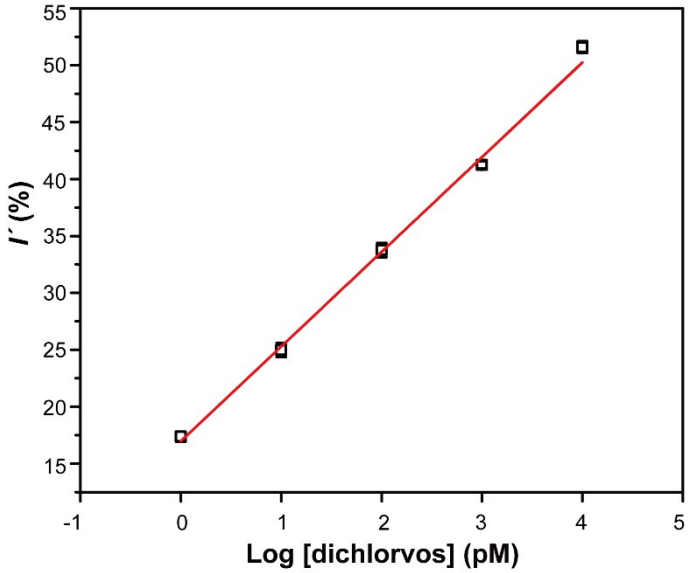

Figure S9 The calibration plot by plotting the inhibition rate (I' %) and the logarithm of dichlorvos concentration.

10. Comparison of performance of different AChE inhibition-based electrochemical biosensors

Table S1 Comparison of performance of different AChE inhibition-based electrochemical biosensors.

Biosensor	Immobilization of AChE	Technique	Pesticide	Linear range	LOD	Ref.
AChE-chitosan/Graphdiyne/3D hierarchical peony-like CoNi-O nanosheets/GCE	Adsorption	DPV	Omethoate	0.47 pM~0.47μM	0.033 pM	5
AChE/3D porous polydopamine-capped AuPt hydrogels/GCE	Entrapment	DPV	Paraoxon-ethyl	0.5~1000 ng L^{-1} (1.8 pM~3.6 nM)	0.185 ng L^{-1} (0.67 pM)	6
AChE/Ni-doped Co/CoO/NC/ CPE	Adsorption	DPV	Paraoxon	10^{-13}~10^{-10} g.mL^{-1} (0.36~3600 μM)	4.6×10^{-14} g.mL^{-1} (1.67 nM)	7
AChE/WO_3/g-C_3N_4/PGE	Covalent binding	CV	Phosmet	5~800 nM	3.6 nM	8
AChE/nitrogen doped carbon dots/BSA/PGE	Covalent binding	CV	Diazinon	10~250 nM	8.9 nM	9
AChE/sponge-like $CuInS_2$ microsphere/rGO/SPCE	Covalent binding	LSV	Chlorpyrifos	0.5~470 ng mL^{-1} (1.4 nM~1.32 μM)	0.023 ng mL^{-1} (0.064 nM)	10
AChE/chitosan-SnS_2/GCE	Adsorption	DPV	Chlorpyrifos	0.02~20000 nM	0.02 nM	11
AChE/Cys/anisotropic gold nanorod/MOF/ITO	Covalent binding	CV	Chlorpyrifos	30~600 ng L^{-1} (0.084~1.68 nM)	3 ng L^{-1} (8.4 pM)	12
AChE/TiO_2-Nanorods/AuNPs/CS&rGO/GCE	Adsorption	DPV	Dichlorvos	2.26~565 nM	2.23 nM	13
AChE/nitrogen-doped graphdiyne/GCE	Covalent binding	DPV	Dichlorvos	10~1000 μg L^{-1} (45 nM~4.5 μM)	1.1 μg L^{-1} (4.95 nM)	14
AChE-$Cu_3(PO_4)_2$ HNF/AuNP/GO/GCE	Biomineralization	SWV	Dichlorvos	1 pM~1 mM	0.07 pM	This work

References

1 Y.-T. Lin, C.-W. Huang, Y.-H. Wang and J. C. S. Wu, *Top. Catal.*, 2020, **63**, 1240-1250.

2 T. Szabó, O. Berkesi, P. Forgó, K. Josepovits, Y. Sanakis, D. Petridis and I. Dékány, *Chem. Mater.*, 2006, **18**, 2740-2749.

3 C. D. Zangmeister, *Chem. Mater.*, 2010, **22**, 5625-5629.

4 H. Liu, L. Zhang, Y. Guo, C. Cheng, L. Yang, L. Jiang, G. Yu, W. Hu, Y. Liu and D. Zhu, *J. Mater. Chem.*, 2013, **1**, 3104-3109.

5 Y. S. Zhao, X. L. Li, J. M. Chen, X. Lu, Y. X. Yang, D. D. Song and F. M. Gao, *Sens. Actuators, B*, 2022, **352**, 131072.

6 Y. Wu, L. Jiao, W. Xu, W. Gu, C. Zhu, D. Du and Y. Lin, *Small*, 2019, **15**, 1900632.

7 Y. Q. An, S. Y. Dong, Z. X. He, Q. Xie and T. L. Huang, *Microchem. J.*, 2022, **172**, 106942.

8 S. Bilal, M. Mudassir Hassan, M. Fayyaz ur Rehman, M. Nasir, A. Jamil Sami and A. Hayat, *Food Chem.*, 2021, **346**, 128894.

9 S. Bilal, A. J. Sami, A. Hayat and M. F. U. Rehman, *Bioelectrochemistry*, 2022, **144**, 107999.

10 T. Itsoponpan, C. Thanachayanont and P. Hasin, *Sens. Actuators, B*, 2021, **337**, 129775.

11 X. Liu, R. Sakthivel, W.-C. Liu, C.-W. Huang, J. Li, C. Xu, Y. Wu, L. Song, W. He and R.-J. Chung, *Food Chem.*, 2020, **324**, 126889.

12 Chansi, P. R. R, I. Mukherjee, T. Basu and L. M. Bharadwaj, *Nanoscale*, 2020, **12**, 21719-21733.

13 J. H. Zhang, H. Y. Hu and L. Q. Yang, *Microchem. J.*, 2021, **168**, 106435.

14 K. Niu, J. Gao, L. X. Wu, X. B. Lu and J. P. Chen, *Anal. Chem.*, 2021, **93**, 8656-8662.